Inorganic Chemistry

pubs.acs.org/IC Article

Using Redox-Active Ligands to Generate Actinide Ligand Radical Species

Shane S. Galley, Scott A. Pattenaude, Debmalya Ray, Carlo Alberto Gaggioli, Megan A. Whitefoot, Yusen Qiao, Robert F. Higgins, W. L. Nelson, Ryan Baumbach, Joseph M. Sperling, Matthias Zeller, Tyler S. Collins, Eric J. Schelter, Laura Gagliardi, Thomas E. Albrecht-Schönzart, and Suzanne C. Bart*

Cite This: *Inorg. Chem.* 2021, 60, 15242−15252 Read Online

ACCESS | Metrics & More | Article Recommendations | Supporting Information

ABSTRACT: Using a redox-active dioxophenoxazine ligand, DOPO (DOPO = 2,4,6,8-tetra-*tert*-butyl-1-oxo-1*H*-phenoxazine-9-olate), a family of actinide (U, Th, Np, and Pu) and Hf tris(ligand) coordination compounds was synthesized. The full characterization of these species using ^{1}H NMR spectroscopy, electronic absorption spectroscopy, SQUID magnetometry, and X-ray crystallography showed that these compounds are analogous and exist in the form $M(DOPO^q)_2(DOPO^{sq})$, where two ligands are of the oxidized quinone form ($DOPO^q$) and the third is of the reduced semiquinone ($DOPO^{sq}$) form. The electronic structures of these complexes were further investigated using CASSCF calculations, which revealed electronic structures consistent with metals in the +4 formal oxidation state and one unpaired electron localized on one ligand in each complex. Furthermore, f orbitals of the early actinides show a sizable bonding overlap with the ligand 2p orbitals. Notably, this is the first example of a plutonium−ligand radical species and a rare example of magnetic data being recorded for a homogeneous plutonium coordination complex.

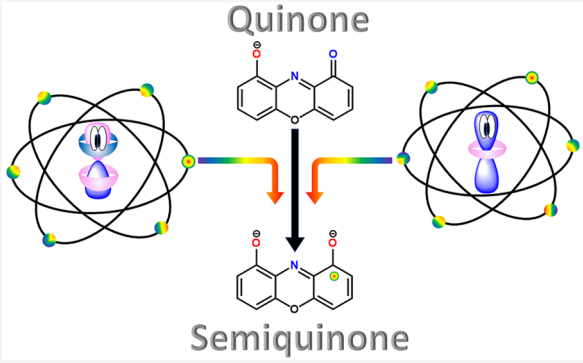

■ INTRODUCTION

Actinides appear in numerous areas within the nuclear fuel cycle; therefore, a fundamental understanding of their chemistry is essential.[1,2] The cycle itself centers around uranium and plutonium processing and enrichment, but the minor actinides (Np, Am, and Cm) are the leading problem in spent fuel due to their higher radioactivities and separations issues. Thus, insight into the bonding and reactivity of these elements could facilitate spent fuel separations and obviate problems associated with the storage, treatment, and disposal of these materials. A useful strategy is to study these elements in a series, which highlights small differences in bonding trends as the actinide series is traversed.

Actinides have been studied extensively for their nuclear properties, but in comparison to the rest of the periodic table the bonding trends and coordination chemistry of these elements are not well understood. This is due, in part, to the fact that few molecular actinide systems extending past thorium and uranium have been established.[3−6] In one such study, tris(cyclopentadienyl) trivalent actinide systems were explored for 5f elements, extending all the way to californium; however, the characterization of these heavier actinide congeners is lacking.[7−11] Similarly, the dipicolinic acid (DPA)[12] and dithiocarbamate or phenanthroline[5] derivatives have been established, but those pertain only to the heavier actinides (Am−Cf) and omit the lighter derivatives.

Besides the challenges of working with highly radioactive material, a considerable obstacle in the generation of a complete actinide series is that the earlier actinides tend to exist in different oxidation states and adapt new morphologies as compared to their later actinide counterparts.[13,14] Moreover, these earlier actinides (Th−Pu) have been established to show small amounts of covalent character in their metal−ligand bonds due to the mixing of energetically similar 6p, 6d, and 5f orbitals.[15,16,1,2] Another challenge is that earlier actinides are prone to disproportionation under aqueous conditions; this can be mitigated by adjusting the environment to nonaqueous and anaerobic conditions, enabling one oxidation state to be probed systematically.[17,18]

Series or families of metals are often amenable to study using redox-active ligands because these ligands stabilize various metal ion oxidation states in highly delocalized systems while remaining isostructural in the ligand environment. These ligands are known for covalent bonding with transition metals, making them of interest for exploring actinide covalency as

Received: June 11, 2021
Published: September 27, 2021

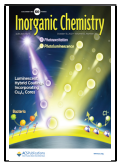

Downloaded via FLORIDA STATE UNIV on November 30, 2021 at 16:11:39 (UTC).
See https://pubs.acs.org/sharingguidelines for options on how to legitimately share published articles.

ACS Publications © 2021 American Chemical Society

https://doi.org/10.1021/acs.inorgchem.1c01766
Inorg. Chem. 2021, 60, 15242−15252

well. Of particular interest is the dioxophenoxazine (DOPO) (DOPO = 2,4,6,8-tetrta-*tert*-butyl-1-oxo-1*H*-phenoxazin-9-olate)[19] ligand, which has been studied with first-row transition metals,[20] main group metals,[21] and lanthanides.[22,23] This ligand is attractive as it can exist in three different oxidation states, namely, the monoanionic quinone ($DOPO^q$) state, the dianionic semiquinone ($DOPO^{sq}$) state, and the trianionic catecholate, ($DOPO^{cat}$) state (Figure 1).[24] This redox

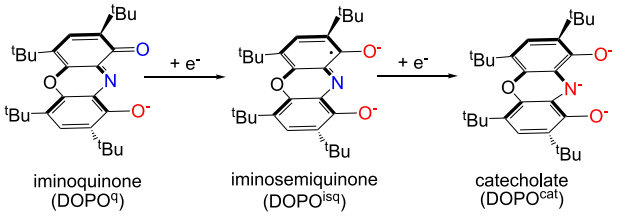

Figure 1. Reduction properties of the DOPO ligand. Red indicates atoms that will form anionic bonds to metals, and blue indicates atoms that will form dative bonds to metals.

flexibility allows the metals to be in their thermodynamically preferred oxidation state while potentially offering the ability to engage in covalent bonding. Thus, if it were possible to make covalent (i.e., delocalized) systems with actinides, electron-rich metals would be ideal.

This hypothesis led us to study the synthesis of trivalent derivatives of the DOPO ligand set of the form $M(DOPO^q)_3$ (M = Ce, Gd, Nd, Sm, Am, Cf, and Bk).[4] These studies focused on the lanthanides and the heavier actinides (Am−Cf), as these metals prefer the trivalent oxidation state. The aim of this study was to compare and contrast the electronic structures of the lanthanide and actinide derivatives. Because lanthanides are known for their ionic bonding, these species would be an ideal baseline to look for degrees of covalent bonding among the actinides. Interestingly, these studies showed that all derivatives had very similar electronic structures, with the majority of the bonding being ionic in nature. While this was predictable for the majority of this family, it was surprising to note that the californium derivative did not show increased covalency when bonding to the ligands, which is in contrast to previous reports of $Cf(HDPA)_3$ (HDPA = 2,6-pyridinedicarboxylate).[12]

Given the lack of covalency in the trivalent system, our attention next turned to the lighter actinides. In contrast to the heavier actinides, the lighter actinides (Th−Pu) can access higher oxidation states more easily due to their increased reducing ability. Therefore, it is possible that the lighter actinides could easily reduce the $DOPO^q$ ligands, creating a more delocalized system with larger degrees of covalent bonding. Herein, we report a series of tetravalent coordination compounds featuring the tris(dioxophenoxazine) framework with Th, U, Np, Pu, and Hf. We postulated that this series would facilitate a comparison of structural and electronic trends across the actinides (Th, U, Np, and Pu) with a transition metal comparison (Hf). These complexes were synthesized, isolated, and fully characterized by structural, spectroscopic, and magnetic techniques in tandem with electronic structure theory calculations.

■ RESULTS AND DISCUSSION

Synthesis. Based on previous work from our laboratory in the synthesis of the trivalent $M(DOPO^q)_3$ (M = Ce, Nd, Sm, Gd, Am, Bk, and Cf) lanthanide and actinide derivatives, the first experiment was aimed at the synthesis of the analogous uranium derivative. Treating a stirring pyridine solution of $UI_3(THF)_4$ with 3 equiv of $HDOPO^q$ generated a dark green solution (Figure 2). After filtration to remove pyridinium

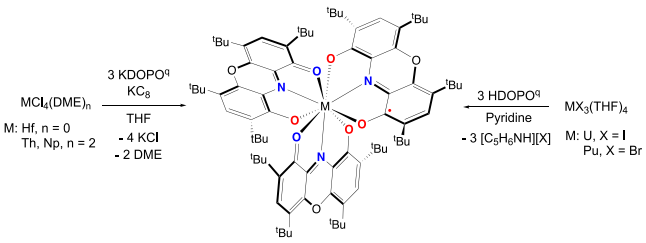

Figure 2. Syntheses of tetravalent DOPO derivatives.

iodide, the volatiles were removed in vacuo, leaving a dark green residue tentatively asssigned as $U(DOPO)_3$. Given that the oxidation states of the ligands were not known prior to characterization, the "DOPO" abbreviation for the ligand will be used in the description in each case until the characterization is described.

This synthetic method was adapted for use with plutonium by significantly scaling down the reaction due to the radioactivity and availability of plutonium starting materials. Treating 5 mg of $PuBr_3(THF)_4$ with 3 equiv of $HDOPO^q$ in pyridine generated a dark blue solution (Figure 2). Workup furnished the desired plutonium derivative $Pu(DOPO)_3$.

With the successful synthesis of the uranium and plutonium congeners, the scope of this chemistry was expanded to target thorium and hafnium derivatives for comparison. Since the common starting materials for these metals are available as tetravalent chlorides, an alternative synthetic method was developed (Figure 2). To solutions of $ThCl_4(DME)_2$ and $HfCl_4$ in THF was added 3 equiv of the potassiated ligand salt, $KDOPO^q(THF)$. Subsequently, 1 equiv of the KC_8 reductant was added to the reaction flask. In each case, a color change from dark blue to dark green ensued. Following workup, $Th(DOPO)_3$ and $Hf(DOPO)_3$ were isolated as solids and characterized further.

After establishing this synthetic pathway for thorium and hafnium, this method was applied to neptunium. As for plutonium, the neptunium synthesis requires the scaling down of the reaction (Figure 2). In an analogous matter, this synthesis was accomplished with 10 mg of $NpCl_4(DME)_2$ in THF using 3 equiv of $KDOPO^q(THF)$ and 1 equiv of KC_8, generating $Np(DOPO)_3$ after workup and the drying of the volatiles.

Given that these derivatives are tris(ligand) compounds, by charge balance it would be predicted that one of the ligands in each compound is reduced by a second electron, forming the semiquinone resonance form of the ligand that features a ligand radical. With two monoanionic ligands and one dianionic ligand, this formulation would support a tetravalent ion.

^{1}H NMR Spectroscopy. ^{1}H NMR spectroscopy is a useful tool in identifying and assessing the purity of these paramagnetic species. Work by our group and others has demonstrated that ^{1}H NMR spectroscopy can be used to identify ligand radicals, as protons in proximity to the unpaired electrons are shifted significantly from their diamagnetic reference values.[4,25,26]

https://doi.org/10.1021/acs.inorgchem.1c01766
Inorg. Chem. 2021, 60, 15242−15252

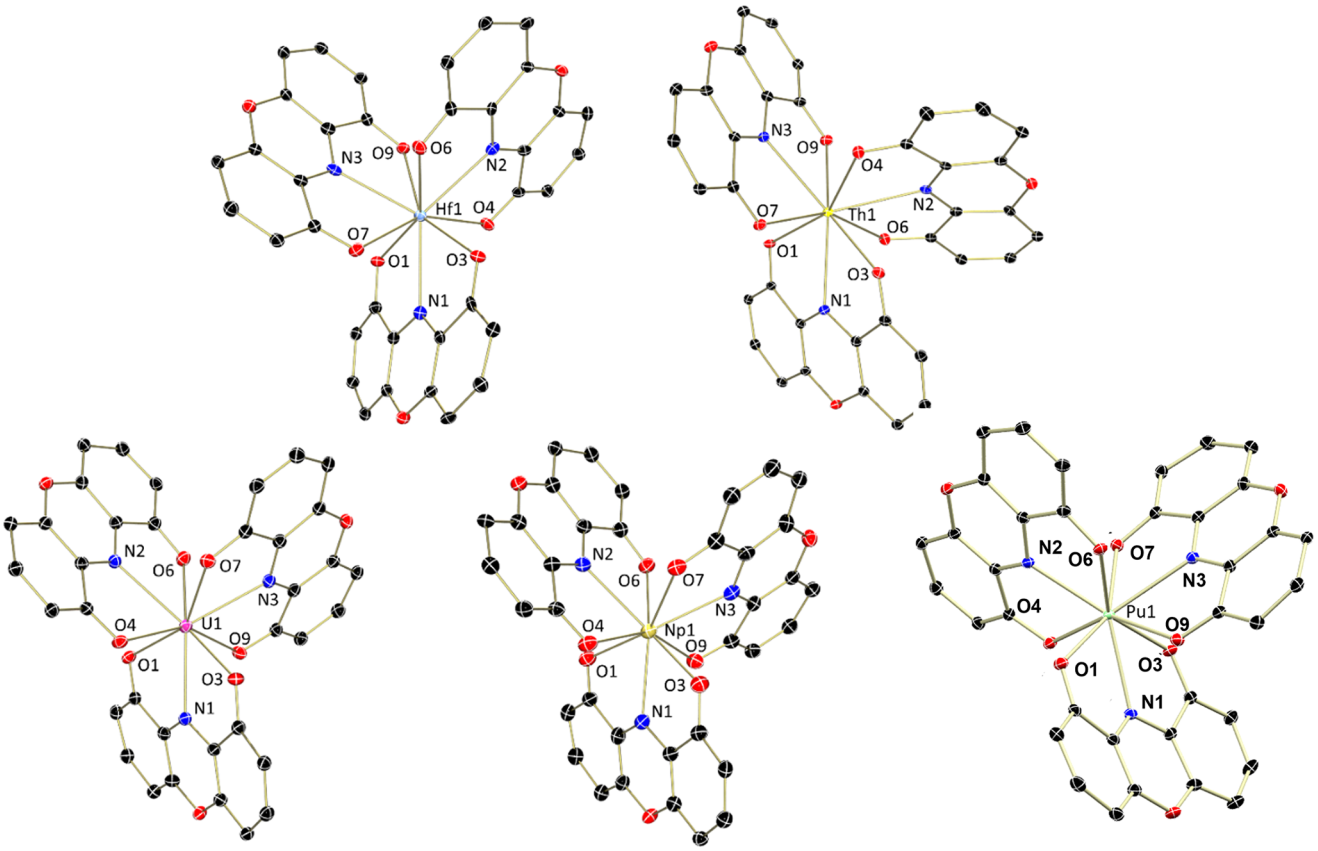

Figure 3. Molecular structures of Hf(DOPO^{q})$_2$(DOPO^{sq}), Th(DOPO^{q})$_2$(DOPO^{sq}), U(DOPO^{q})$_2$(DOPO^{sq}), Np(DOPO^{q})$_2$(DOPO^{sq}), and Pu(DOPO^{q})$_2$(DOPO^{sq}) shown with 30% probability ellipsoids. Hydrogen atoms, *tert*-butyl groups, and cocrystallized solvent molecules have been omitted for clarity.

Table 1. Metal−Ligand Bond Distances (Å) for Ln/An DOPO Complexes[a]

	Hf	Th	U	Np	Pu
M−O1	2.237 (3)	2.453 (3)	2.307 (4)	2.360 (5)	2.3434 (17)
M−N1	2.346 (4)	2.640 (3)	2.430 (5)	2.553 (6)	2.5428 (19)
M−O3	2.253 (3)	2.480 (3)	2.349 (4)	2.416 (5)	2.4001 (17)
M−O4	**2.167 (3)**	**2.365 (3)**	**2.248 (4)**	**2.301 (5)**	**2.2886 (17)**
M−N2	**2.258 (3)**	**2.524 (4)**	**2.529 (5)**	**2.414 (6)**	**2.4122 (19)**
M−O6	**2.159 (3)**	**2.372 (3)**	**2.276 (4)**	**2.282 (5)**	**2.2890 (17)**
M−O7	2.253 (3)	2.480 (3)	2.330 (4)	2.402 (5)	2.3869 (16)
M−N3	2.343 (4)	2.647 (4)	2.497 (4)	2.558 (6)	2.538 (2)
M−O9	2.250 (3)	2.486 (3)	2.337 (4)	2.419 (5)	2.4253 (16)

[a]Those bolded are assigned as the semiquinone ligand.

The ^{1}H NMR spectrum (benzene-d_6, 25 °C) of paramagnetic U(DOPO)$_3$ showed resonances at 0.45 and 1.52 ppm (54H each), which were assigned as the protons of the *tert*-butyl groups, as well as a broad shifted singlet at −82.80 ppm (6H), which was assigned as the protons on the aryl rings. The number and integration values of these resonances support the formation of a symmetric product in solution, which is expected. The significantly shifted aryl resonance is indicative of a semiquinone ligand, which is consistent with the formula U(DOPO^{q})$_2$(DOPO^{sq}) for a tetravalent ion.

In the cases of the thorium and hafnium derivatives, the ^{1}H NMR spectra were also recorded. However, these spectra were not helpful for the structural assignment as they were extremely broad, with inconsistent numbers of resonances. Given that these metals are generally in their +4 state, i.e., f^0 (thorium), or d^0 (hafnium) electron configurations, the broad spectra were indicative of paramagnetism, which could only come from a ligand radical. Thus, these species were tentatively assigned as Th(DOPO^{q})$_2$(DOPO^{sq}) and Hf(DOPO^{q})$_2$(DOPO^{sq}). Due to concerns with the increased radioactivity of the neptunium and plutonium derivatives, NMR spectroscopic data were not obtainable.

X-ray Crystallography. Allowing pyridine solutions of all these new dioxophenoxazine derivatives to stand over approximately 1 h produced crystals suitable for single crystal X-ray diffraction. Analysis of these crystals confirmed the molecular structures of all derivatives as tris(ligand) chelates with nine coordinate metal ions (Figure 3, metrical parameters are shown in Table 1). An examination of the metrical parameters of these structures showed variations among the ligands within each complex, supporting that different ligand oxidation states are likely present in the solid state. Previous

https://doi.org/10.1021/acs.inorgchem.1c01766
Inorg. Chem. 2021, 60, 15242−15252

studies from our group have demonstrated that the metal–ligand bond distances of uranium derivatives are effective indicators of ligand reduction and the oxidation state,[25−27] which will be applied here.

In the case of uranium, which crystallized in the $P2_1/c$ space group, the U−O bond lengths range from 2.307(4) to 2.349(4) Å on two of the ligands, which is the average of an anionic and dative uranium bond. This is expected based on the DOPO^q resonance form. The third ligand shows contracted U−O bonds that are out of the range for the quinone ligand with distances of 2.248(4) and 2.276(4) Å, supporting two anionic U−O bonds for the DOPO^{sq} ligand. This is corroborated by the U−O distances of tetravalent (DOPO^{sq})UI_2(THF)[24] of 2.203(4) and 2.231(4) Å, a molecule which has been established to contain a semiquinone ligand. These findings from crystallography support the previous assignment as U(DOPO^q)$_2$(DOPO^{sq}).

The intraligand distances are also a useful metric for probing ligand reduction; to quantify this, Brown and co-workers have developed the metrical oxidation state (MOS) model for ONO ligands (Table 2).[19] This model describes the degree of π-bonding based on distances obtained from X-ray crystallography and provides a MOS value that is indicative of the oxidation state (with negative value). The values for the species studied here and those of the previously established Nd(DOPO^q)$_3$ are listed in Table 2. In the case of Nd(DOPO^q)$_3$, all ligands are in the quinone form and have MOS values of −0.98, −1.01, and −1.11, which are consistent with this oxidation state. The investigation of the intraligand bond distances in tris(dioxo-phenoxazine) uranium using the MOS method shows that the two quinone ligands have MOS values of −1.59 and −1.70, which are slightly higher than expected; however, the ligand oxidation state is corroborated by the other metrical parameters and additional characterization data. The third ligand has a MOS value of −2.19, which is consistent with the semiquinone variant and confirms the formula as U(DOPO^q)$_2$(DOPO^{sq}).

Table 2. Metrical Oxidation State (MOS) Values for Ligands in Tris(dioxophenoxazine) Complexes[a]

compound	DOPO (*a*)	DOPO (*b*)	DOPO (*c*)
Nd	−0.98	−1.01	−1.11
U	−1.59	−1.70	−2.19
Np	−1.03	−1.21	−2.13
Pu	−1.21	−1.22	−2.06
Hf	−1.13	−1.16	−1.95
Th	−1.44	- 1.26	−2.12

[a]Nd(DOPO^q)$_3$ is shown for reference.

The molecular structures of the plutonium derivative displayed similar phenomena as U(DOPO^q)$_2$(DOPO^{sq}), which crystallized in the $P2_1/c$ space group. The Pu−O bond lengths for two of the ligands range from 2.3434(17) to 2.4253(16) Å, and also is consistent with the DOPO^q formulation (Table 1). These distances are similar to those noted for the Pu−carbonates in $[Na_6Pu(CO_3)_5]_2 \cdot Na_2CO_3 \cdot 33H_2O$, which range from 2.381(6) to 2.430(6) Å.[28] The third ligand exhibited contracted Pu−O bond lengths of 2.2886(17) and 2.2890(17) Å. In comparison to a N,O-donor β-ketoiminate system, $Pu^{IV}(^{Ar}acnac)_4$ (Ar = 3,5-^{t}Bu$_2$C$_6$H$_3$),[29] the Pu^{IV} center has Pu−O distances of 2.177(10) and 2.197(8) Å, which are consistent with the semiquinone derivative.

The MOS model for intraligand distances shows that the pair of ligands are in the quinone resonance form with values of −1.21 and −1.22, whereas the third ligand has a MOS value of −2.06, supporting the semiquinone form of the ligand in Pu(DOPO^q)$_2$(DOPO^{sq}) (Table 2).

X-ray diffraction studies showed the tris(chelate) system to be the same for Hf, Th, and Np, with the same phenomenon of a change of the ligand oxidation state of DOPO^q to DOPO^{sq} for one of the ligands. Hf(DOPO^q)$_2$(DOPO^{sq}) crystallizes in the $P2_1/n$ space group with Hf−O bond lengths that range from 2.237(3) to 2.53(3) Å for the quinone ligands, and these ligands have MOS values of −1.13 and −1.16. The reduction of the third ligand causes a decrease in the Hf−O bond distances to 2.159(3) and 2.167(3) Å, which is consistent with semiquinone formation. For comparison, Rothwell reports a Hf−O(phenoxide) bond of 1.926(3) Å in HfCl(OC$_6$H$_3$^{t}Bu$_2$-2,6)$_3$.[30] That in the dioxophenoxazine hafnium compound is slightly longer, likely due to the extreme sterics imparted by the 12 *tert*-butyl groups. The MOS value of −1.95 corresponds to the Hf−O distances, confirming the semiquinone formulation of Hf(DOPO^q)$_2$(DOPO^{sq}).

As with hafnium, Th(DOPO^q)$_2$(DOPO^{sq}) crystallizes in the same space group. The Th−O distances range from 2.453(3) to 2.486(3) Å for the pair of quinone ligands, with a decrease in the lengths of these bonds to 2.365(3) and 2.372(3) Å following reduction to DOPO^{sq} (Table 1). For comparison, the length of the Th−O(phenoxide) bond in Th(*O*-2,6-^{t}Bu$_2$C$_6$H$_3$)$_4$ has been established to be 2.189(4) Å.[31] As with Hf, the Th−O bonds for the DOPO^{sq} ligand species are longer due to the extreme steric hindrance imparted by the *tert*-butyl groups.[3] The MOS model corresponds well these data (Table 2), as the values for the quinone ligands are −1.44 and −1.26 while that for the semiquinone ligand is −2.12, consistent with the assignment as Th(DOPO^q)$_2$(DOPO^{sq}).

The final example is that of neptunium, which resides between uranium and plutonium on the Periodic Table. The same trend holds for neptunium as for both of its neighbors. Np(DOPO^q)$_2$(DOPO^{sq}) crystallizes in the $P2_1/c$ space group. The Np−O bond distances range from 2.360(5) to 2.558 (6) Å for the pair of ligands assigned as the quinones, and these distances decrease to 2.282(5) and 2.301(5) Å upon the reduction to the semiquinone form. Although this difference is not as substantial as in other cases, there is a small change as would be expected. For reference, the Np−O distances in Np[^{Ar}OSeO^{Ar}]$_2$(THF)$_2$ (^{Ar}OSeO^{Ar} = [(4,6-^{t}Bu$_2$C$_6$H$_2$O)$_2$Se]$^{2-}$) range from 2.168(9) to 2.228(11) Å,[32] whereas that in Cp$_3$NpOPh was found to be 2.136(7) Å.[33] Again, the large size of the dioxophenoxazine ligand likely plays a role in the slight discrepancy in distances. The MOS model supports the ligand oxidation states as well, with values of −1.03 and −1.21 for the quinone ligands and −2.13 for the semiquinone ligand.

Electronic Absorption Spectroscopy. The electronic absorption spectroscopic properties of the M(DOPO^q)$_2$(DOPO^{sq}) (M = U, Np, and Pu) family were explored to help gain insight into the electronic structures of its members (Figure 4). In the cases of the dioxophenoxazine derivatives, the high molar absorptivity of this redox-active ligand dominates these spectra. In each case, the absorptions arising at 416−422 and 741−753 nm are indicative of DOPO^q species from the π-to-π^* electron absorptions. These absorptions are analogous to those observed in the previously reported trivalent series where only DOPO^q ligands were

https://doi.org/10.1021/acs.inorgchem.1c01766
Inorg. Chem. 2021, 60, 15242−15252

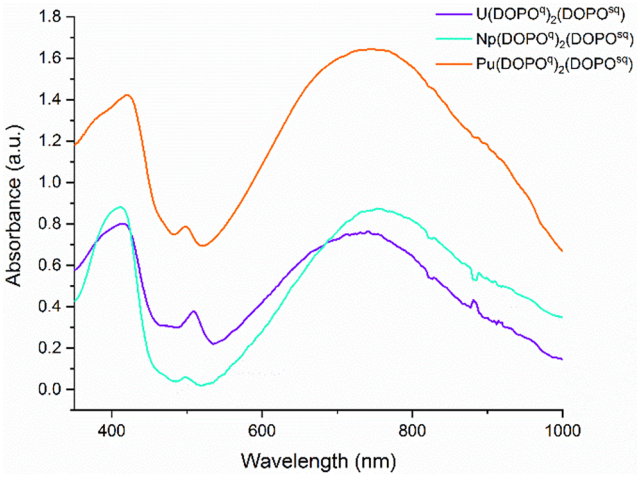

Figure 4. Solid-state electronic absorption spectra for U-$(DOPO^q)_2(DOPO^{sq})$, Np$(DOPO^q)_2(DOPO^{sq})$, and Pu-$(DOPO^q)_2(DOPO^{sq})$ acquired from 350 to 1000 nm.

present. Compared to this homoleptic system, the spectra acquired for the tetravalent system feature a new absorption at 504−512 nm, which can be assigned to the semiquinone ligand that contains the radical. Like the trivalent system, the absorbances around 730, 753, and 745 nm are responsible for the dark green color of these powders. Solution data for M$(DOPO^q)_2(DOPO^{sq})$ (M = Th and Hf) show spectra with analogous features (Figure S2).

Magnetometry Studies. Variable-temperature and field-dependent magnetic measurements (2 K) were performed to further support the ligand and metal oxidation states in the M$(DOPO^q)_2(DOPO^{sq})$ (M = U, Th, Hf, and Pu) family (Figure 5). In the case of the uranium derivative, the following two possible formal electronic configurations were proposed: (a) U(IV)$(DOPO^q)_2(DOPO^{sq})$, which was supported by the solid-state data, and (b) U(VI)$(DOPO^{sq})_3$, which would be symmetric in the solid state. At room temperature, the μ_{eff} value for the uranium derivative was 2.93 μ_B, which is consistent with reported magnetic data for tetravalent $(DOPO^{sq})UI_2(THF)_2$[24] and other uranium(IV) complexes that include one (S = 1/2) ligand radical.[25,26,34] The temperature dependence of the μ_{eff} value for this molecule follows a monotonic decrease, indicating the depopulation of ligand field levels due to the uranium cation.[35−38] The μ_{eff} value at 2 K is 1.42 μ_B, which is smaller than the expected spin-only magnetic moment of one ligand radical (1.73 μ_B) but comparable to the magnetic moment of other uranium(IV) complexes bearing ligand radicals, including $(^{Mes}PDI^{Me})UI_3$.[24] Therefore, the magnetic moment at 2 K was attributed to a magnetic singlet U(IV) cation and a ligand-based doublet. Overall, the magnetic measurements indicate the spin state as a $5f^2$ U(IV) and a S = 1/2 $DOPO^{sq}$ radical (case a) rather than a $5f^0$ U(VI) and three S = 1/2 $DOPO^{sq}$ radicals (case b). Moreover, field-dependent data at 2 K reached 0.74 μ_B at 7 T (Figure S6), supporting the assignment of one unpaired electron per molecule at a low temperature, namely, U(IV)-$(DOPO^q)_2(DOPO^{sq})$.[4−7]

The thorium and hafnium derivatives differ from uranium as Th and Hf are generally found in the +4 oxidation state. As $5f^0$ and $5d^0$ metals, respectively, they are diamagnetic. In these cases, these species should display a magnetic behavior consistent with only one unpaired spin in the ligand. Analysis

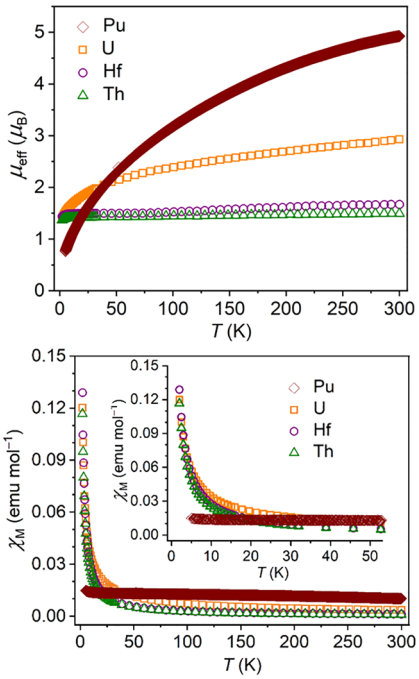

Figure 5. Variable-temperature magnetic susceptibility data for U$(DOPO^q)_2(DOPO^{sq})$, Th$(DOPO^q)_2(DOPO^{sq})$, Hf-$(DOPO^q)_2(DOPO^{sq})$, and Pu$(DOPO^q)_2(DOPO^{sq})$ in Bohr magnetons (μ_B) (top) and χ_M (bottom) units. The inset in the bottom plot displays a smaller temperature range.

reveals effective magnetic moments of 1.44 and 1.37 μ_B for the hafnium and thorium cases, respectively, at 2 K (Figure 5). Although these magnetic moments are lower than the spin-only value for one unpaired electron, these are consistent with what would be expected for a ligand radical, supporting the formulation of the M(IV)$(DOPO^q)_2(DOPO^{sq})$ electronic structure. There is little change in these magnetic moments throughout the temperature range, indicating that the radical stays constant, which is as expected.

The plutonium derivative, Pu$(DOPO^q)_2(DOPO^{sq})$, was also analyzed to confirm the presence of the ligand radical. These measurements were done separately due to the higher levels of radioactivity associated with this element. While magnetic measurements of transuranium elements are rare compared to those of their Th and U counterparts, in this case the magnetic properties were important to establish as, to our knowledge, this is the first plutonium species with a ligand radical. Additionally, very little magnetic data have been reported for homogeneous monomeric plutonium coordination compounds,[39−41] meaning this example will serve as a useful comparison for future work.

As in the cases for the U, Th, and Hf analogous, the Pu compound was measured across a temperature range from 2 to 300 K in the solid state. As for uranium, there are two main resonance structures here that can be considered. The first is consistent with the experimental data as Pu-$(DOPO^q)_2(DOPO^{sq})$, which features a plutonium(IV) ion and a ligand radical. This would mean four 5f electrons for plutonium plus a ligand radical for a total of five unpaired electrons. The second case to consider is the resonance structure with a Pu(III) ion and no ligand radical—a $5f^5$ system. The effective magnetic moment at high temperature (300 K) of ∼4.8 μ_B is consistent with the first case, as the

https://doi.org/10.1021/acs.inorgchem.1c01766
Inorg. Chem. 2021, 60, 15242−15252

Pu(IV) ion is expected to have magnetic properties in the context of j−j coupling (due to the strong spin−orbit interaction). With four unpaired electrons on plutonium(IV) plus one on the ligand, this would be a $S = 5/2$ system. If this were a Pu(III) ion with no ligand radical, there would also be five unpaired electrons in the system; thus, room temperature magnetic data are not useful for discerning between these possibilities. However, the effective magnetic moment is as expected for five unpaired electrons in an actinide system.[1] Additionally, the presence of the ligand radical is supported by ligand structural parameters as well as Pu−O distances as determined by crystallography.

At a low temperature, the effective magnetic moment of ∼0.75 μ_B was observed for Pu(DOPO^q)$_2$(DOPO^{sq}) (Figure 5). Examples of magnetic moments determined for molecular plutonium species at low temperatures are lacking, making the meaning behind this value more difficult to interpret. Considering the first resonance structure with Pu(IV) and a ligand radical, it would be expected that the Pu ion would behave similarly to the uranium example, where at low temperatures the Pu ground state is $S = 0$, reflecting a low magnetic moment. Because the magnetic moment observed at low temperatures is not close to 0 μ_B, it is possible to conclude the presence of the ligand radical at this temperature. This is supported by the fact that in Pu(COT)$_2$, Pu(IV) was found to be diamagnetic in the temperature range from 4.2 to 45 K, as it has a $^5I_4$ ground state.[40] Recent work from the Gagliardi lab corroborates this finding.[41] Their studies have shown that due to spin orbit coupling in the Pu(IV) ion, the $J = 4$ term splits into nine states, and the ligand field stabilizes the $^5I_0$ ground state. At low temperatures, the amount of thermal energy precludes the population of these excited states; thus, the magnetic properties reflect the $^5I_0$ state.

In the other scenario with a Pu(III) ion with five unpaired f electrons, previous work has established a moment for KPu(COT)$_2$·2THF of 1.25 μ_B at a low temperature, featuring a $^6H_{5/2}$ sextet ground state.[39] The moment agrees with the free-ion moment for Pu(III) with intermediate coupling taken into account. Because the moment observed for Pu(DOPO^q)$_2$(DOPO^{sq}) is lower than that for the free Pu(III) ion, which would be the case if there were no ligand radical, the best formulation for this compound is as a Pu(IV)−ligand radical species.

Computational Studies. To gain further insight into the electronic structure, we used computational methods to analyze the electronic properties of all the metal−DOPO complexes. For the Np−DOPO derivative, a CASSCF calculation with an active space of eight electrons in 12 orbitals was carried out. The active-space natural orbitals of the Np−DOPO complex together with the occupation numbers (Figure 6) clearly show two π orbitals (and two π^* orbitals) on the ligands together with the f orbitals on Np and one orbital delocalized on the other ligand. The sum of the occupation number on Np is 2.99 electrons, which is consistent with a formal oxidation state of +4. The other unpaired electron is mainly localized on a nitrogen center in one of the DOPO ligands. These results suggest an electronic structure in which the neptunium exists as a +4 f^3 ion together with two DOPO ligands in the monoanionic quinone state (DOPO^q) and one DOPO ligand in the dianionic semiquinone state (DOPO^{sq}).

Next, the spin-state energetics were analyzed (Table S11). The quintet and triplet spin states are within 0.2 (using CASSCF) and 0.3 kcal/mol (using CASPT2) of each other.

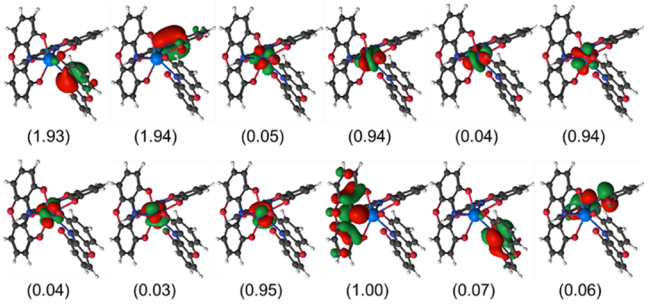

Figure 6. Active-space orbitals of the quintet spin state of the Np−DOPO complex (occupation numbers are in brackets).

The singlet state is higher in energy by ∼33.3 kcal/mol and ∼23.3 kcal/mol when using the CASSCF and CASPT2 levels of theory, respectively, compared to the quintet and triplet states (Table S11). In the CASSCF method, the quintet state is more stable, whereas using CASPT2 shows that the triplet state is more stable. Further, Mulliken spin density analyses (see Table S12) reveal that in the triplet state Np and the radical N center on the ligand are antiferromagnetically coupled. From the orbital pictures in the quintet spin states, we do not see any covalency between the metal and ligand orbitals. However, in the triplet spin state, which is almost degenerate to the quintet spin state (active orbitals in Figure S9), there is a sizable covalency between the unpaired electron on the DOPO ligand and one f orbital on Np. Furthermore, we analyzed the multireference character of the wave function for different spin states of the metal−DOPO complexes. As shown in Table S13, the dominant electronic configuration in the quintet spin state for Np−DOPO is $\pi_1^2 \pi_2^2 f_1^0 f_2^{1u} f_3^0 f_4^{1u} f_5^0 f_6^0 f_7^{1u} \pi_3^{1u} \pi_4^0 \pi_5^0$. However, for the triplet and singlet spin states the largest configurations have weights below 40%, indicating the clear multiconfigurational character. A similar behavior was observed for all the other metal−DOPO complexes (see Table S13), where all spin states except the highest one have the multiconfigurational character.

For the U−DOPO complex, a CASSCF calculation with an active space of seven electrons in 12 orbitals was performed. The active-space orbitals of the U-DOPO complex (in the quartet spin state, Figure S7) together with their occupation numbers show that the number of electrons in the U f orbitals is 2.0, which is consistent with a +4 oxidation state. An unpaired electron on one DOPO ligand was also observed, indicating the same electronic structure as that for Np−DOPO. In total, U−DOPO has three unpaired electrons. The spin-state analyses revealed that the quartet and doublet states are close to each other, within 0.1 kcal/mol using the CASSCF method and within 0.5 kcal/mol using CASPT2 method (Table S11). Because the energy difference between the quartet and doublet states is less than 1 kcal/mol (i.e., within the limit of the computational accuracy), one can consider both spin states as degenerate. In the doublet spin state, the radical N center on the ligand is antiferromagnetically coupled to the U center (Table S12). From the orbitals in the quartet spin state, a sizable covalency between the metal and the ligands was not noted. However, in the doublet state (active orbitals in Figure S8), some covalency between the DOPO radical ligand and one f orbital of the metal was evident.

For the Pu−DOPO complex, the active space orbitals of the Pu-DOPO complex as determined from a CASSCF(9,12) calculation are presented in Figure S10. The sextet and quartet

https://doi.org/10.1021/acs.inorgchem.1c01766
Inorg. Chem. 2021, 60, 15242−15252

spin states are nearly degenerate (i.e., within 0.3 and 0.1 kcal/mol using CASSCF and CASPT2, respectively (Table S11)). The doublet spin state is 44.1 and 37.6 kcal/mol higher in energy when using CASSCF and CASPT2 levels of theory when compared to those of the sextet and quartet states (Table S12). Analogously to U−DOPO and Np−DOPO, the Mulliken spin density analysis of the quartet state of Pu−DOPO also shows antiferromagnetic coupling between the radical N center on the ligand and the Pu center. The orbital picture for the sextet spin state does not show any covalency between the metal and the ligand, but in the quartet spin state (Figure S11) the electron on one DOPO ligand orbital where the unpaired electron resides is mixed with one f orbital on Pu, inducing some covalency.

The analyses for Th−DOPO and Hf−DOPO complexes also reveal that the unpaired electron is localized on one of the DOPO ligands in each case, mostly centered on the N of the ligand. The Mulliken spin density difference is almost zero on the metal centers, confirming the closed-shell nature of the Th(IV) and Hf(IV) ions. The active-space orbitals (together with their occupation numbers) of Th−DOPO and Hf−DOPO are shown in Figures S12 and S13, respectively.

In each case, the computational analyses support the tetravalency of the metals in this family of derivatives and show that there is electron spin density localized on one ligand in each complex through the occupation of π^*-orbitals. Thus, the best formulation for these derivatives is as M-$(DOPO^q)_2(DOPO^{sq})$, where each complex supports two quinone ligands and one semiquinone ligand. This finding supports the experimental data, which were corroborated through multiple techniques. Specifically, X-ray crystallography shows one reduced ligand in each case, which is evident from the distortions in the corresponding structural parameters. This charge is clearly relegated to one ligand and it is not delocalized to the other ligands, as indicated by starkly different metrical parameters.

■ CONCLUSIONS

In summation, a redox-active dioxophenoxazine ligand has been used to generate a new family of tris(ligand) metal complexes, where M = U, Th, Np, Pu, and Hf. Using a combination of spectroscopic, structural, magnetic, and computational techniques, these species have all been established to have analogous electronic structures. In each case, X-ray crystallography supports the presence of a ligand radical based on structural parameters, and the magnetic data support tetravalent metal centers with ligand radicals. The computational results confirm this electronic structural assignment, and these complexes can best be thought of as $M(IV)(DOPO^q)_2(DOPO^{sq})$.

This work captures a rare series of nonaqueous early actinide (and Hf)−ligand complexes that are all tetravalent in nature and all contain a ligand radical. Although uranium and thorium species have been well established to support such electronic structures, this is new for neptunium and plutonium. Additionally, the magnetic data obtained for plutonium are quite rare. This study goes well with other studies that highlight a comparison of the bonding in tetravalent transition metals with early actinides, which analyze both structural and computational data.[14,42]

Our previous work with the same ligand system where $M(DOPO^q)_3$ (M = Am, Cf, and Bk) were generated shows that early actinides prefer tetravalency, while the later actinides show trivalency. Additionally, the earlier actinides are reducing enough to generate and stabilize ligand radicals. Computational work in this study revealed that certain spin states of each of these early actinide examples show true covalency, where ligand orbitals overlap significantly with f orbitals just as d orbitals do with ligand orbitals in transition metal organometallic complexes.

■ EXPERIMENTAL SECTION

General Considerations. All manipulations were performed using standard Schlenk techniques or in an MBraun inert atmosphere drybox with an atmosphere of either purified nitrogen (Hf, Th, and U) or ultrahigh purity argon (transuranics). Hafnium(IV) chloride (99.9%), was purchased from Strem Chemicals and used as received. Pentane, tetrahydrofuran, and toluene were dried and deoxygenated using literature procedures with a Seca solvent purification system.[43] Anhydrous pyridine was purchased from Sigma-Aldrich and was used without further purification. Benzene-d_6 was purchased from Cambridge Isotope Laboratories, degassed by three freeze−pump−thaw cycles, and dried over molecular sieves and sodium. 2,4,6,8-Tetra-*tert*-butyl-9-hydroxy-1*H*-phenoxazin-1-one ($HDOPO^q$),[19] potassium 2,4,6,8-tetra-*tert*-butyl-9-hydroxy-1*H*-phenoxazin-1-one ($KDOPO^q$),[24] potassium graphite,[44] $U[N(SiMe_3)_2]_3$,[45] $ThCl_4(DME)$,[46] $UI_3(THF)_4$,[47] $NpCl_4(DME)_2$,[48] and $PuBr_3(THF)_4$[49] were prepared according to literature procedures.

Caution! ^{232}Th,^{238}U,^{237}Np, ^{239}Pu, and ^{242}Pu represent serious health risks due to their α-emission and the radiotoxicity associated with their α-, β-, and γ- emitting daughters. All studies with these transuranic elements were conducted in a laboratory dedicated to studies on transuranic elements. This laboratory is located in a nuclear science facility at Florida State University and is equipped with HEPA-filtered hoods and gloveboxes. A series of instruments continually monitor the radiation levels in the laboratory. All free-flowing actinide solids are handled in gloveboxes, and products are only examined when coated with immersion or Krytox oil. Significant limitations exist to accurately determining yields of these actinide compounds because drying, isolating, and weighing a solid is required, which creates an inhalation hazard and manipulation difficulties given the small quantities of products from these reactions.

NMR Spectroscopy. Where possible, ^1H NMR spectra were recorded on a Varian Inova 300 spectrometer at 299.992 MHz. All chemical shifts are reported relative to the peak for $SiMe_4$ using ^1H (residual) chemical shifts of the solvent as a secondary standard. The spectra for paramagnetic molecules were obtained using an acquisition time of 0.5 s; thus, the peak widths reported have an error of ±2 Hz. For paramagnetic molecules, the ^1H NMR spectroscopic data are reported with the chemical shift, followed by the peak width at the half height in Hertz, the integration value, and the peak assignment where possible.

Crystallography. Single crystals of $Hf(DOPO^q)_2(DOPO^{sq})$ were coated with polybutenes and quickly transferred to the goniometer head of a Nonius Kappa CCD diffractometer. equipped with an Oxford Cryosystems low-temperature device. Examination and data collection were performed with Mo Kα radiation (λ = 0.71073 Å) at 100 K using Nonius Collect software. The data were processed using HKL3000 and data were corrected for absorption and scaled using Scalepack.

Single crystals of $Th(DOPO^q)_2(DOPO^{sq})$ were coated with polybutenes and quickly transferred to the goniometer head of a Bruker Quest diffractometer with κ-geometry, an I-μ-S microsource X-ray tube, a laterally graded multilayer (Goebel) mirror single crystal for monochromatization, a Photon-II CMOS area detector, and an Oxford Cryosystems low-temperature device. Examination and data collection were performed with Cu Kα radiation (λ = 1.54178 Å) at 100 K.

Single crystals of $U(DOPO^q)_2(DOPO^{sq})$, $Np(DOPO^q)_2(DOPO^{sq})$, and $Pu(DOPO^q)_2(DOPO^{sq})$ were mounted on MiTiGen mounts with krytox oil, and the crystals were optically aligned on a Bruker ApexII X-ray diffractometer using a built-in

https://doi.org/10.1021/acs.inorgchem.1c01766
Inorg. Chem. 2021, 60, 15242−15252

camera. Preliminary measurements were performed using an I-μ-S X-ray source (Mo Kα, λ= 0.71073 A) with high-brilliance and high-performance focusing quest multilayer optics. APEXIII software was used for solving the unit cells, data collection, and integration. PLATON was used to finalize the structure for any issues. CIF files are available from the Cambridge Crystallographic Data Centre (CCDC) under nos. 2050818 (Hf), 2050819 (Th), 2050820 (U), 2050821 (Np), and 2050822 (Pu).

Electronic Absorption Spectroscopy. Electronic absorption spectroscopic measurements were recorded at 294 K with a Craic Technologies microspectrophotometer. Single crystals of each compound were placed on a quartz slide in immersion oil, and the data were collected from 300 to 1100 nm. Solution electronic absorption spectroscopic measurements were recorded at 294 K in sealed 1 cm quartz cuvettes with a Cary 6000i UV−vis-NIR spectrophotometer.

SQUID Magnetometry. Magnetic data were collected on a Quantum Design magnetic property measurement system (MPMS-7). Temperature-dependent data were collected under applied 1 T DC fields from 2 to 300 K, and field-dependent data were performed at 2 K with applied magnetic field strengths that varied from 0 to 7 T. Corrections for the intrinsic diamagnetism of the samples were made using Pascal's constants.[50]

Each magnetism sample was prepared in the glovebox and placed in a heat-sealed compartment of a plastic drinking straw. The plastic drinking straws were evacuated overnight prior to use. These straws were then sealed at one end (∼9.5 cm from the top) by heating a pair of forceps and crimping the sides of the straw until the two sides were fused together. The microcrystalline compound (10−20 mg) was loaded into the straw, capped with <10 mg of quartz wool (dried at 250 °C prior to use), and packed in tightly using a Q-tip. The other end of the plastic drinking straw was then sealed directly above the quartz wool, forming a small compartment (<1 cm). The sample and quartz wool were massed four times each to the nearest 0.1 mg, and the values used were the averages of these mass measurements.

Computational Methods. For the computational study, we used the experimental structures of metal−DOPO complexes, replaced the *t*-butyl groups with hydrogen atoms, and optimized only the geometries of those hydrogen atoms with unrestricted density functional theory (DFT) using the ADF2016 software package,[51−53] employing the B3LYP functional.[54,55] A TZP quality basis was used for the metals, while a DZP quality basis was employed for the other atoms (H, C, O, and N). Scalar relativistic effects were included by means of the zeroth-order regular approximation (ZORA) to the Dirac equation.[56,57]

Electronic structures of the metal−DOPO complexes are complicated due to their multiconfigurational nature. Thus, electronic structures of metal−DOPO complexes were analyzed using the single-point complete active space self-consistent field (CASSCF)[58] method as implemented in the Openmolcas software package.[59] All-electron ANO-RCC-VTZP basis sets[60] were used on metal centers and the six oxygen and three nitrogen centers directly bonded to the metal centers. The ANO-RCC-VDZ basis set was used for C, H, and the three oxygen centers that are not directly bonded to the metal centers. For U, Np, and Pu, an (n,12) active space was used (where n = 7, 8, and 9 for U, Np, and Pu respectively); for Hf and Th, a (5,5) active space was used. In the cases of U, Np, and Pu, all seven 5f-orbitals of the metals, two π-orbitals, the correlating π^* orbitals of the ligands, and one singly occupied π orbital containing the radical electron were included in the active space. Hf and Th are d^0 systems in their +4 oxidation state. Thus, for these systems we only included ligand orbitals in the active space. Further relative energies of various spin states were computed using the CASSCF method. To recover the dynamic correlation on the spin state ordering, we also performed second-order perturbation theory calculations on top of the CASSCF reference wave functions (CASPT2)[61,62] for U, Np, and Pu DOPO complexes. To account for the intruder state problem, we used an imaginary shift of 0.2 au and an IPEA shift of 0.25 au in CASPT2 calculations. Scalar relativistic effects were included using the Douglas−Kroll−Hess Hamiltonian. Resolution of identity Cholesky decomposition (RICD)[63] was used for all the calculations to decrease the computational cost of the two electron integrals evaluation.

Preparation of Hf(DOPO^q)$_2$(DOPO^{sq}). A 20 mL scintillation vial was charged with $HfCl_4$ (0.010 g, 0.031 mmol) and 5 mL of THF. A solution of KDOPO^q (THF) (0.058 g, 0.106 mmol) dissolved in 5 mL of THF was added to the vial, causing a color change from blue to green. To the vial was added 1 equiv of KC_8 (0.005 g, 0.037 mmol), and the solution was allowed to stir for 1 h before it was concentrated in vacuo. The resulting green powder was extracted into toluene, filtered to remove KCl and graphite, and concentrated in vacuo to a dark green powder assigned as Hf(DOPO^q)$_2$(DOPO^{sq}). Single crystals for X-ray crystallography were grown from a concentrated pyridine solution at room temperature. Analysis for $C_{84}H_{114}N_3O_9Hf$: Calcd C, 67.79; H, 7.82; N, 2.71. Found: C, 69.69; H, 8.69; N, 2.72. ^{1}H NMR (C_6D_6, 25 °C): δ (s, 1.52), (s,2.08), (s, 2.73).

Preparation of Th(DOPO^q)$_2$(DOPO^{sq}). A 20 mL scintillation vial was charged with $ThCl_4(DME)_2$ (0.084 g, 0.152 mmol) and 5 mL of THF. A solution of KDOPO^q (THF) (0.250 g, 0.456 mmol) dissolved in 5 mL of THF was added to the vial, causing a color change from blue to green. To the vial was added 1 equiv of KC_8 (0.021 g, 0.155 mmol), and the solution was allowed to stir for 1 h before it was concentrated in vacuo. The resulting green powder was extracted into toluene, filtered to remove KCl and graphite, and concentrated in vacuo to a dark green powder assigned as Th(DOPO^q)$_2$(DOPO^{sq}). Single crystals for X-ray crystallography were grown from a concentrated pyridine solution at room temperature. Analysis for $C_{84}H_{114}N_3O_9Th$: Calcd C, 65.43; H, 7.45; N, 2.73. Found: C, 64.51; H, 7.80; N, 2.57. ^{1}H NMR (C_6D_6, 25 °C): δ (s, 1.23), (s, 0.98).

Preparation of U(DOPO^q)$_2$(DOPO^{sq}). A 7 mL scintillation vial was charged with $UI_3(THF)_4$ (0.005 g, 0.0104 mmol) and 2 mL of pyridine. A solution of HDOPO^q (0.0135 g, 0.0311 mmol) dissolved in 2 mL of pyridine was added to the vial, causing a color change from purple to dark green. Upon standing, dark green block crystals suitable for X-ray analysis formed and were immediately analyzed.

Alternative Route to the Preparation of U(DOPO^q)$_2$(DOPO^{sq}). A 20 mL scintillation vial was charged with $U[N(SiMe_3)_2]_3$ (0.025 g, 0.035 mmol) and 5 mL of THF. A solution of HDOPO^q (0.046 g, 0.105 mmol) in 5 mL of THF was slowly added to the stirring solution of $U[N(SiMe_3)_2]_3$, resulting in a color change from violet to green. After stirring for 1 h, the volatiles were removed in vacuo, resulting in a green powder (0.051 g, 0.033 mmol, 94%) that was assigned as U(DOPO^q)$_2$(DOPO^{sq}). Green crystals suitable for X-ray analysis were grown by slow evaporation from pentane over a week at room temperature. Analysis for $C_{84}H_{114}N_3O_9U$: Calcd C, 65.18; H, 7.42; N, 2.71. Found: C, 65.07; H, 7.28; N, 2.82. ^{1}H NMR (C_6D_6, 25 °C): δ −82.80 (38, 6H, Ar−CH), 0.45 (3, 54H, $-C(CH_3)_3$), 1.52 (4, 54H, $-C(CH_3)_3$).

Preparation of Np(DOPO^q)$_2$(DOPO^{sq}). A 20 mL scintillation vial was charged with $NpCl_4(DME)_2$ (0.010 g, 0. 0.0178 mmol) and 2 mL of THF. A solution of KDOPO^q (THF) (0.009 g, 0.0178 mmol) dissolved in 2 mL of THF was added to the vial, causing a color change from blue to green. To the vial was added 1 equiv of KC_8 (0.002 g, 0.0178 mmol), and the solution was allowed to stir for 1 h before it was concentrated in vacuo. The residue was dissolved in 2 mL of pyridine. The resulting green solution was allowed to stand overnight to produce single crystals suitable for X-ray crystallography.

Preparation of Pu(DOPO^q)$_2$(DOPO^{sq}). A 7 mL scintillation vial was charged with pale blue hydrated $^{239}PuBr_3$ (0.005 g, 0.0104 mmol) and 2 mL of pyridine. A solution of HDOPO^q (0.0135 g, 0.0311 mmol) dissolved in 2 mL of pyridine was added to the vial, causing a color change to dark green-blue. Overnight, dark block crystals suitable for X-ray analysis formed and were immediately analyzed.

■ ASSOCIATED CONTENT

Supporting Information

The Supporting Information is available free of charge at https://pubs.acs.org/doi/10.1021/acs.inorgchem.1c01766.

Experimental procedures, characterization data, copies of spectroscopic data, and computational analysis (PDF)

Accession Codes

CCDC 2050818−2050822 contain the supplementary crystallographic data for this paper. These data can be obtained free of charge via www.ccdc.cam.ac.uk/data_request/cif, or by emailing data_request@ccdc.cam.ac.uk, or by contacting The Cambridge Crystallographic Data Centre, 12 Union Road, Cambridge CB2 1EZ, UK; fax: +44 1223 336033.

■ AUTHOR INFORMATION

Corresponding Author

Suzanne C. Bart − *H. C. Brown Laboratory, Department of Chemistry, Purdue University, West Lafayette, Indiana 47907, United States;* orcid.org/0000-0002-8918-9051; Email: sbart@purdue.edu

Authors

Shane S. Galley − *H. C. Brown Laboratory, Department of Chemistry, Purdue University, West Lafayette, Indiana 47907, United States;* orcid.org/0000-0003-0679-6567

Scott A. Pattenaude − *H. C. Brown Laboratory, Department of Chemistry, Purdue University, West Lafayette, Indiana 47907, United States;* orcid.org/0000-0002-0564-2796

Debmalya Ray − *Department of Chemistry, Supercomputing Institute, and Chemical Theory Centre, University of Minnesota, Minneapolis, Minnesota 55455, United States;* orcid.org/0000-0002-8309-8183

Carlo Alberto Gaggioli − *Department of Chemistry, Pritzker School of Molecular Engineering, James Franck Institute, and Chicago Center for Theoretical Chemistry, The University of Chicago, Chicago, Illinois 60637, United States;* orcid.org/0000-0001-9105-8731

Megan A. Whitefoot − *H. C. Brown Laboratory, Department of Chemistry, Purdue University, West Lafayette, Indiana 47907, United States*

Yusen Qiao − *P. Roy and Diana T. Vagelos Laboratories, Department of Chemistry, University of Pennsylvania, Philadelphia, Pennsylvania 19104, United States;* orcid.org/0000-0001-7654-8636

Robert F. Higgins − *P. Roy and Diana T. Vagelos Laboratories, Department of Chemistry, University of Pennsylvania, Philadelphia, Pennsylvania 19104, United States*

W. L. Nelson − *National High Magnetic Field Laboratory, Florida State University, Tallahassee, Florida 32310, United States; Department of Physics, Florida State University, Tallahassee, Florida 32306, United States*

Ryan Baumbach − *National High Magnetic Field Laboratory, Florida State University, Tallahassee, Florida 32310, United States; Department of Physics, Florida State University, Tallahassee, Florida 32306, United States*

Joseph M. Sperling − *Department of Chemistry and Biochemistry, Florida State University, Tallahassee, Florida 32306, United States;* orcid.org/0000-0003-1916-5633

Matthias Zeller − *H. C. Brown Laboratory, Department of Chemistry, Purdue University, West Lafayette, Indiana 47907, United States;* orcid.org/0000-0002-3305-852X

Tyler S. Collins − *H. C. Brown Laboratory, Department of Chemistry, Purdue University, West Lafayette, Indiana 47907, United States;* orcid.org/0000-0003-1026-4379

Eric J. Schelter − *P. Roy and Diana T. Vagelos Laboratories, Department of Chemistry, University of Pennsylvania, Philadelphia, Pennsylvania 19104, United States;* orcid.org/0000-0002-8143-6206

Laura Gagliardi − *Department of Chemistry, Pritzker School of Molecular Engineering, James Franck Institute, and Chicago Center for Theoretical Chemistry, The University of Chicago, Chicago, Illinois 60637, United States;* orcid.org/0000-0001-5227-1396

Thomas E. Albrecht-Schönzart − *Department of Chemistry and Biochemistry, Florida State University, Tallahassee, Florida 32306, United States;* orcid.org/0000-0002-2989-3311

Complete contact information is available at: https://pubs.acs.org/10.1021/acs.inorgchem.1c01766

Author Contributions

The manuscript was written through contributions of all authors.

Notes

The authors declare no competing financial interest.

■ ACKNOWLEDGMENTS

This work was funded by the Division of Chemical Sciences, Geosciences, and Biosciences, Office of Basic Energy Sciences of the U.S. Department of Energy through Grants DESC0008479 (S.C.B.), DE-SC002183 (L.G.), DEFG02-13ER16414 (T.E.A.S.), and DE-SC0017259 (E.J.S.). D.R., C.A.G, and L.G. used resources of the Minnesota Supercomputing Institute to perform all the calculations. Acquisition of the plutonium magnetic data was supported by the Center for Actinide Science and Technology (CAST), which is an Energy Frontier Research Centre (EFRC) funded by the U.S. Department of Energy (DOE), Office of Science, Basic Energy Sciences (BES) under Award DE-SC0016568. Work done by R.B. was performed at the National High MAgnetic Field LAboratory, which is supported by the National Science Foundation Cooperative Agreement No. DMR-1644779 and the State of Florida. The X-ray diffractometer at Purdue University used for structure determination of **1-Hf**, **1-U**, and **1-Th** was funded by the National Science Foundation through the Major Research Instrumentation Program under Grant CHE 1625543. We also thank Prof. Jay Kikkawa (UPenn Physics) for assistance with the magnetic measurements.

■ REFERENCES

(1) Katz, J. J.; Morss, L. R.; Seaborg, G. T. *The Chemistry of the Actinide Elements*, 2nd ed.; Chapman Hall: New York, NY, 1986.

(2) Nash, K. L.; Nilsson, M., Introduction to the Reprocessing and Recycling of Spent Nuclear Fuels. In *Reprocessing and Recycling of Spent Nuclear Fuel*; Taylor, R., Ed.; Woodhead Publishing: Cambridge, U.K., 2015; pp 3−25.

(3) Gaunt, A. J.; Neu, M. P. Recent Developments in Nonaqueous Plutonium Coordination Chemistry. *C. R. Chim.* **2010**, *13*, 821−831.

(4) Galley, S. S.; Pattenaude, S. A.; Gaggioli, C. A.; Qiao, Y.; Sperling, J. M.; Zeller, M.; Pakhira, S.; Mendoza-Cortes, J. L.; Schelter, E. J.; Albrecht-Schmitt, T. E.; Gagliardi, L.; Bart, S. C. Synthesis and Characterization of Tris-chelate Complexes for Understanding f-Orbital Bonding in Later Actinides. *J. Am. Chem. Soc.* **2019**, *141*, 2356−2366.

(5) Cary, S. K.; Su, J.; Galley, S. S.; Albrecht-Schmitt, T. E.; Batista, E. R.; Ferrier, M. G.; Kozimor, S. A.; Mocko, V.; Scott, B. L.; Van Alstine, C. E.; White, F. D.; Yang, P. A Series of Dithiocarbamates for Americium, Curium, and Californium. *Dalton Trans.* **2018**, *47*, 14452−14461.

(6) Cary, S. K.; Vasiliu, M.; Baumbach, R. E.; Stritzinger, J. T.; Green, T. D.; Diefenbach, K.; Cross, J. N.; Knappenberger, K. L.; Liu, G.; Silver, M. A.; DePrince, A. E.; Polinski, M. J.; Van Cleve, S. M.; House, J. H.; Kikugawa, N.; Gallagher, A.; Arico, A. A.; Dixon, D. A.; Albrecht-Schmitt, T. E. Emergence of Californium as the Second Transitional Element in the Actinide Series. *Nat. Commun.* **2015**, *6*, 6827.

(7) Baumgärtner, F.; Fischer, E. O.; Kanellakopulos, B.; Laubereau, P. Tri(cyclopentadienyl)americium(III). *Angew. Chem., Int. Ed. Engl.* **1966**, *5*, 134−135.

(8) Laubereau, P. G.; Burns, J. H. *Tricyclopentadienyl Complexes of Promethium, Curium, Berkelium, and Californium: Their Preparation and Identification by Microtechniques*; CONF-700403; Oak Ridge National Laboratory: Oak Ridge, TN, 1971.

(9) Su, J.; Windorff, C. J.; Batista, E. R.; Evans, W. J.; Gaunt, A. J.; Janicke, M. T.; Kozimor, S. A.; Scott, B. L.; Woen, D. H.; Yang, P. Identification of the Formal + 2 Oxidation State of Neptunium: Synthesis and Structural Characterization of $\{Np^{II}[C_5H_3(SiMe_3)_2]_3\}^{1-}$. *J. Am. Chem. Soc.* **2018**, *140*, 7425−7428.

(10) Windorff, C. J.; MacDonald, M. R.; Meihaus, K. R.; Ziller, J. W.; Long, J. R.; Evans, W. J. Expanding the Chemistry of Molecular U^{2+} Complexes: Synthesis, Characterization, and Reactivity of the $\{[C_5H_3(SiMe_3)_2]_3U\}^-$ Anion. *Chem. - Eur. J.* **2016**, *22*, 772−782.

(11) Woen, D. H.; Evans, W. J. Expanding the +2 Oxidation State of the Rare-Earth Metals, Uranium, and Thorium in Molecular Complexes. In *Handbook on the Physics and Chemistry of Rare Earths*, Vol. *50*; Bünzli, J.-C. G., Pecharsky, V. K., Eds.; Elsevier, 2016; pp 337−394.

(12) Albrecht-Schmitt, T. Californium Gleaming. *Nat. Chem.* **2014**, *6*, 840−840.

(13) Cary, S. K.; Galley, S. S.; Marsh, M. L.; Hobart, D. L.; Baumbach, R. E.; Cross, J. N.; Stritzinger, J. T.; Polinski, M. J.; Maron, L.; Albrecht-Schmitt, T. E. Incipient Class II Mixed Valency in a Plutonium Solid-State Compound. *Nat. Chem.* **2017**, *9*, 856−861.

(14) Behrle, A. C.; Myers, A. J.; Kerridge, A.; Walensky, J. R. Coordination Chemistry and QTAIM Analysis of Homoleptic Dithiocarbamate Complexes, $M(S_2CN^iPr_2)_4$ (M = Ti, Zr, Hf, Th, U, Np). *Inorg. Chem.* **2018**, *57*, 10518−10524.

(15) Kaltsoyannis, N. Does Covalency Increase or Decrease across the Actinide Series? Implications for Minor Actinide Partitioning. *Inorg. Chem.* **2013**, *52*, 3407−3413.

(16) Neidig, M. L.; Clark, D. L.; Martin, R. L. Covalency in F-Element Complexes. *Coord. Chem. Rev.* **2013**, *257*, 394−406.

(17) Choppin, G. R.; Bond, A. H.; Hromadka, P. M. Redox Speciation of Plutonium. *J. Radioanal. Nucl. Chem.* **1997**, *219*, 203−210.

(18) Rao, L. F.; Choppin, G. R. Kinetics of the Reduction of Neptunium(VI) by Dicarboxylic Acids. *Inorg. Chem.* **1984**, *23*, 2351−2354.

(19) Ranis, L. G.; Werellapatha, K.; Pietrini, N. J.; Bunker, B. A.; Brown, S. N. Metal and Ligand Effects on Bonding in Group 6 Complexes of Redox-Active Amidodiphenoxides. *Inorg. Chem.* **2014**, *53*, 10203−10216.

(20) Ivakhnenko, E. P.; Starikov, A. G.; Minkin, V. I.; Lyssenko, K. A.; Antipin, M. Y.; Simakov, V. I.; Korobov, M. S.; Borodkin, G. S.; Knyazev, P. A. Synthesis, Molecular and Electronic Structures of Six-Coordinate Transition Metal (Mn, Fe, Co, Ni, Cu, and Zn) Complexes with Redox-Active 9-Hydroxyphenoxazin-1-One Ligands. *Inorg. Chem.* **2011**, *50*, 7022−7032.

(21) Romanenko, G. V.; Ivakhnenko, E. P.; Minkin, V. I.; Starikov, A. G.; Bogomyakov, A. S.; Veber, S. L. Sn(IV) Complexes with Bi- and Tridentate Phenoxazin-1-One Ligands: Synthesis, Structure and Magnetic Properties. *Inorg. Chim. Acta* **2014**, *418*, 66−72.

(22) Ivakhnenko, E. P.; Romanenko, G. V.; Simakov, V. I.; Knyazev, P. A.; Bogomyakov, A. S.; Lyssenko, K. A.; Minkin, V. I. Synthesis and Structure of Nonacoordinated Tris-chelate Lanthanide (III) Complexes with Tridentate 2,4,6,8-Tetrakis(Tert-Butyl)-9-Hydroxyphenoxazin-1-One Ligands. *Inorg. Chim. Acta* **2017**, *458*, 116−121.

(23) Ivakhnenko, E. P.; Simakov, V. I.; Knyazev, P. A.; Romanenko, G. V.; Bogomyakov, A. S.; Minkin, V. I. Synthesis and Structure of a Tris-chelate Gd^{III} Complex with Tridentate 2,4,6,8-Tetrakis(Tert-Butyl)-9-Hydroxyphenoxazinone Ligands. *Mendeleev Commun.* **2016**, *26*, 49−51.

(24) Pattenaude, S. A.; Kuehner, C. S.; Dorfner, W. L.; Schelter, E. J.; Fanwick, P. E.; Bart, S. C. Spectroscopic and Structural Elucidation of Uranium Dioxophenoxazine Complexes. *Inorg. Chem.* **2015**, *54*, 6520−6527.

(25) Anderson, N. H.; Odoh, S. O.; Williams, U. J.; Lewis, A. J.; Wagner, G. L.; Lezama Pacheco, J.; Kozimor, S. A.; Gagliardi, L.; Schelter, E. J.; Bart, S. C. Investigation of the Electronic Ground States for a Reduced Pyridine(diimine) Uranium Series: Evidence for a Ligand Tetraanion Stabilized by a Uranium Dimer. *J. Am. Chem. Soc.* **2015**, *137*, 4690−4700.

(26) Anderson, N. H.; Odoh, S. O.; Yao, Y.; Williams, U. J.; Schaefer, B. A.; Kiernicki, J. J.; Lewis, A. J.; Goshert, M. D.; Fanwick, P. E.; Schelter, E. J.; Walensky, J. R.; Gagliardi, L.; Bart, S. C. Harnessing Redox Activity for the Formation of Uranium Tris(imido) Compounds. *Nat. Chem.* **2014**, *6*, 919−926.

(27) Kraft, S. J.; Williams, U. J.; Daly, S. R.; Schelter, E. J.; Kozimor, S. A.; Boland, K. S.; Kikkawa, J. M.; Forrest, W. P.; Christensen, C. N.; Schwarz, D. E.; Fanwick, P. E.; Clark, D. L.; Conradson, S. D.; Bart, S. C. Synthesis, Characterization, and Multielectron Reduction Chemistry of Uranium Supported by Redox-Active α-Diimine Ligands. *Inorg. Chem.* **2011**, *50*, 9838−9848.

(28) Clark, D. L.; Conradson, S. D.; Keogh, D. W.; Palmer, P. D.; Scott, B. L.; Tait, C. D. Identification of the Limiting Species in the Plutonium(IV) Carbonate System. Solid State and Solution Molecular Structure of the $[Pu(CO_3)_5]^{6-}$ Ion. *Inorg. Chem.* **1998**, *37*, 2893−2899.

(29) Schnaars, D. D.; Gaunt, A. J.; Hayton, T. W.; Jones, M. B.; Kirker, I.; Kaltsoyannis, N.; May, I.; Reilly, S. D.; Scott, B. L.; Wu, G. Bonding Trends Traversing the Tetravalent Actinide Series: Synthesis, Structural, and Computational Analysis of $An^{IV}(^{Ar}acnac)_4$ Complexes (An = Th, U, Np, Pu; ^{Ar}acnac = ArNC(Ph)ChC(Ph)O; Ar = 3,5-$tBu_2C_6H_3$). *Inorg. Chem.* **2012**, *51*, 8557−8566.

(30) Chamberlain, L.; Huffman, J. C.; Keddington, J.; Rothwell, I. P. Crystal and Molecular Structure of Monochlorotris (2,6-di-t-butylphenoxo)hafnium. *J. Chem. Soc., Chem. Commun.* **1982**, 805−806.

(31) Berg, J. M.; Clark, D. L.; Huffman, J. C.; Morris, D. E.; Sattelberger, A. P.; Streib, W. E.; Van der Sluys, W. G.; Watkin, J. G. Early Actinide Alkoxide Chemistry. Synthesis, Characterization, and Molecular Structures of Thorium(IV) and Uranium(IV) Aryloxide Complexes. *J. Am. Chem. Soc.* **1992**, *114*, 10811−21.

(32) Myers, A. J.; Rungthanaphatsophon, P.; Behrle, A. C.; Vilanova, S. P.; Kelley, S. P.; Lukens, W. W.; Walensky, J. R. Structure and Properties of $[(4,6\text{-}tBu_2C_6H_2O)_2Se]_2An(THF)_2$, An = U, Np, and their Reaction with *p*-Benzoquinone. *Chem. Commun.* **2018**, *54*, 10435−10438.

(33) De Ridder, D. J. A.; Apostolidis, C.; Rebizant, J.; Kanellakopulos, B.; Maier, R. Tris(η^5-cyclopentadienyl)-phenolatoneptunium(IV). *Acta Crystallogr., Sect. C: Cryst. Struct. Commun.* **1996**, *52*, 1436−1438.

(34) Castro-Rodriguez, I.; Nakai, H.; Zakharov, L. N.; Rheingold, A. L.; Meyer, K. A Linear, O-Coordinated η^1-CO_2 Bound to Uranium. *Science* **2004**, *305*, 1757−1760.

(35) Castro-Rodriguez, I.; Olsen, K.; Gantzel, P.; Meyer, K. Uranium Tris-Aryloxide Derivatives Supported by Triazacyclononane: Engendering a Reactive Uranium(III) Center with a Single Pocket for Reactivity. *J. Am. Chem. Soc.* **2003**, *125*, 4565−4571.

(36) Lewis, A. J.; Williams, U. J.; Kikkawa, J. M.; Carroll, P. J.; Schelter, E. J. Uranium Pyrrolylamine Complexes Featuring a Trigonal Binding Pocket and Interligand Noncovalent Interactions. *Inorg. Chem.* **2012**, *51*, 37−39.

(37) Lewis, A. J.; Williams, U. J.; Carroll, P. J.; Schelter, E. J. Tetrakis(bis(trimethylsilyl)amido)uranium(IV): Synthesis and Reactivity. *Inorg. Chem.* **2013**, *52*, 7326−7328.

https://doi.org/10.1021/acs.inorgchem.1c01766
Inorg. Chem. 2021, 60, 15242−15252

(38) Kindra, D. R.; Evans, W. J. Magnetic Susceptibility of Uranium Complexes. *Chem. Rev.* **2014**, *114*, 8865−8882.
(39) Karraker, D. G.; Stone, J. A. Bis(cyclooctatetraenyl)neptunium(III) and -plutonium(III) Compounds. *J. Am. Chem. Soc.* **1974**, *96*, 6885−6888.
(40) Karraker, D. G.; Stone, J. A.; Jones, E. R.; Edelstein, N. Bis(cyclooctatetraenyl)neptunium(IV) and Bis(cyclooctatetraenyl)-plutonium(IV). *J. Am. Chem. Soc.* **1970**, *92*, 4841−4845.
(41) Singh, S. K.; Cramer, C. J.; Gagliardi, L. Correlating Electronic Structure and Magnetic Anisotropy in Actinide Complexes [An(cot)$_2$], An$^{III/IV}$ = U, Np, and Pu. *Inorg. Chem.* **2020**, *59*, 6815−6825.
(42) Berryman, V. E. J.; Shephard, J. J.; Ochiai, T.; Price, A. N.; Arnold, P. L.; Parsons, S.; Kaltsoyannis, N. Quantum Chemical Topology and Natural Bond Orbital Analysis of M−O Covalency in M(OC$_6$H5)$_4$ (M = Ti, Zr, Hf, Ce, Th, Pa, U, Np). *Phys. Chem. Chem. Phys.* **2020**, *22*, 16804−16812.
(43) Pangborn, A. B.; Giardello, M. A.; Grubbs, R. H.; Rosen, R. K.; Timmers, F. J. Safe and Convenient Procedure for Solvent Purification. *Organometallics* **1996**, *15*, 1518−1520.
(44) Chakraborty, S.; Chattopadhyay, J.; Guo, W.; Billups, W. E. *Angew. Chem., Int. Ed.* **2007**, *46*, 4486−4488.
(45) Stewart, J. L.; Andersen, R. A. Trivalent Uranium Chemistry: Molecular Structure of [(Me$_3$Si)$_2$N]$_3$U. *Polyhedron* **1998**, *17*, 953−958.
(46) Cantat, T.; Scott, B. L.; Kiplinger, J. L. Convenient Access to the Anhydrous Thorium Tetrachloride Complexes ThCl$_4$(DME)$_2$, ThCl$_4$(1,4-dioxane)$_2$ and ThCl$_4$(THF)$_{3.5}$ Using Commercially Available and Inexpensive Starting Materials. *Chem. Commun.* **2010**, *46*, 919−921.
(47) Clark, D. L.; Sattelberger, A. P.; Andersen, R. A. Lewis Base Adducts of Uranium Triiodide and Tris[bis(trimethylsilyl)amido]-uranium. *Inorg. Synth.* **2007**, *31*, 307−315.
(48) Reilly, S. D.; Brown, J. L.; Scott, B. L.; Gaunt, A. J. Synthesis and Characterization of NpCl$_4$(DME)$_2$ and PuCl$_4$(DME)$_2$ Neutral Transuranic an(IV) Starting Materials. *Dalton Trans.* **2014**, *43*, 1498−1501.
(49) Gaunt, A. J.; Reilly, S. D.; Enriquez, A. E.; Hayton, T. W.; Boncella, J. M.; Scott, B. L.; Neu, M. P. Low-Valent Molecular Plutonium Halide Complexes. *Inorg. Chem.* **2008**, *47*, 8412−8419.
(50) Bain, G. A.; Berry, J. F. Diamagnetic Corrections and Pascal's Constants. *J. Chem. Educ.* **2008**, *85*, 532.
(51) Fonseca Guerra, C.; Snijders, J. G.; te Velde, G.; Baerends, E. J. Towards an Order-N DFT Method. *Theor. Chem. Acc.* **1998**, *99*, 391−403.
(52) Software for Chemistry and Materials (SCM). *Amsterdam Density Functional Theory (ADF)*; SCM: Amsterdam, The Netherlands, 2013.
(53) te Velde, G.; Bickelhaupt, F. M.; Baerends, E. J.; Fonseca Guerra, C.; van Gisbergen, S. J. A.; Snijders, J. G.; Ziegler, T. Chemistry with ADF. *J. Comput. Chem.* **2001**, *22*, 931−967.
(54) Becke, A. D. Density-Functional Thermochemistry. III. The Role of Exact Exchange. *J. Chem. Phys.* **1993**, *98*, 5648−5652.
(55) Lee, C.; Yang, W.; Parr, R. G. Development of the Colle-Salvetti Correlation-Energy Formula into a Functional of the Electron Density. *Phys. Rev. B: Condens. Matter Mater. Phys.* **1988**, *37*, 785−789.
(56) van Lenthe, E.; Baerends, E. J.; Snijders, J. G. Relativistic Total Energy Using Regular Approximations. *J. Chem. Phys.* **1994**, *101*, 9783−9792.
(57) van Lenthe, E.; van Leeuwen, R.; Baerends, E. J.; Snijders, J. G. Relativistic Regular Two-Component Hamiltonians. *Int. J. Quantum Chem.* **1996**, *57*, 281−293.
(58) Roos, B. O.; Taylor, P. R.; Sigbahn, P. E. M. A Complete Active Space SCF Method (CASSCF) Using a Density Matrix Formulated Super-Ci Approach. *Chem. Phys.* **1980**, *48*, 157−173.
(59) Galván, I. F.; Vacher, M.; Alavi, A.; Angeli, C.; Aquilante, F.; Autschbach, J.; Bao, J. J.; Bokarev, S. I.; Bogdanov, N. A.; Carlson, R. K.; Chibotaru, L. F.; Creutzberg, J.; Dattani, N.; Delcey, M. G.; Dong, S. S.; Dreuw, A.; Freitag, L.; Frutos, L. M.; Gagliardi, L.; Gendron, F.; Giussani, A.; González, L.; Grell, G.; Guo, M.; Hoyer, C. E.; Johansson, M.; Keller, S.; Knecht, S.; Kovačević, G.; Källman, E.; Li Manni, G.; Lundberg, M.; Ma, Y.; Mai, S.; Malhado, J. P.; Malmqvist, P. Å.; Marquetand, P.; Mewes, S. A.; Norell, J.; Olivucci, M.; Oppel, M.; Phung, Q. M.; Pierloot, K.; Plasser, F.; Reiher, M.; Sand, A. M.; Schapiro, I.; Sharma, P.; Stein, C. J.; Sørensen, L. K.; Truhlar, D. G.; Ugandi, M.; Ungur, L.; Valentini, A.; Vancoillie, S.; Veryazov, V.; Weser, O.; Wesołowski, T. A.; Widmark, P.-O.; Wouters, S.; Zech, A.; Zobel, J. P.; Lindh, R. Openmolcas: From Source Code to Insight. *J. Chem. Theory Comput.* **2019**, *15*, 5925−5964.
(60) Roos, B. O.; Veryazov, V.; Widmark, P.-O. Relativistic Atomic Natural Orbital Type Basis Sets for the Alkaline and Alkaline-Earth Atoms Applied to the Ground-State Potentials for the Corresponding Dimers. *Theor. Chem. Acc.* **2004**, *111*, 345−351.
(61) Andersson, K.; Malmqvist, P. A.; Roos, B. O.; Sadlej, A. J.; Wolinski, K. Second-Order Perturbation Theory with a CASSCF Reference Function. *J. Phys. Chem.* **1990**, *94*, 5483−5488.
(62) Andersson, K.; Malmqvist, P. Å.; Roos, B. O. Second-Order Perturbation Theory with a Complete Active Space Self-Consistent Field Reference Function. *J. Chem. Phys.* **1992**, *96*, 1218−1226.
(63) Aquilante, F.; Pedersen, T. B.; Lindh, R. Low-Cost Evaluation of the Exchange Fock Matrix from Cholesky and Density Fitting Representations of the Electron Repulsion Integrals. *J. Chem. Phys.* **2007**, *126*, 194106.

https://doi.org/10.1021/acs.inorgchem.1c01766
Inorg. Chem. 2021, 60, 15242−15252